ADVANCES IN ATMOSPHERIC SCIENCES, VOL. 24, NO. 2, 2007, 181–190

Seasonally Varying Reference Atmospheres for East Asia

Byung-Ju SOHN* and Geun-Hyeok RYU

School of Earth and Environmental Sciences, Seoul National University, Seoul 151-747*, Korea*

(Received 16 January 2006; revised 29 June 2006)

ABSTRACT

Vertical profiles of seasonally varying pressure, temperature, water vapor, and trace gases (O_3, N_2O, CO, CH_4), representing atmospheric conditions up to a height of 100 km over the East Asia region (30°–50°N, 110°–150°E) were constructed by using various observation data, model outputs of atmospheric thermodynamic parameters, and gaseous concentrations. Optical characteristics of the obtained East Asia reference atmospheres were compared with those from typical midlatitude summer and winter atmospheres. It was noted that, in the water vapor field, there are major differences between the two model atmospheres during the summer. The resultant impact during the summer of water vapor difference on incoming solar fluxes at the surface and emitted terrestrial fluxes at the top of the atmosphere are 14.3 W m^{-2} and 6.5 W m^{-2}, respectively. On the other hand, the winter difference between East Asian and midlatitude atmospheres appears to be insignificant. Reference atmospheres for the spring and fall are also available. Utilizing the constructed atmospheric profiles as inputs to the radiative transfer model, it is expected that the constructed seasonally varying reference atmospheres can facilitate better descriptions of optical properties in East Asia.

Key words: East Asian reference atmosphere, radiative transfer, atmospheric optical property

DOI: 10.1007/s00376-007-0181-z

1. Introduction

Atmospheric gases interfere with radiation while it propagates within the atmosphere. Longwave radiation energy emitted by the Earth is strongly absorbed by water vapor, ozone, and other greenhouse gases in the atmosphere. On the other hand, the solar radiation reaching the Earth's surface is mainly attenuated by molecular scattering, water vapor, and ozone absorption taking place in the atmosphere (Goody and Yung, 1989; Liou, 2002). Therefore, vertical thermodynamic structures of the atmosphere are essential information for calculating the radiative transfer within the atmosphere (McClatchey et al., 1972), in particular for designing satellite sensors for observing geophysical parameters or developing remote sensing algorithms.

However, because atmospheric conditions vary significantly with time and location, it is common to use a reference atmosphere representing a certain geographic location and season for a radiative transfer calculation, from which general characteristics related to atmospheric radiation or observing sensors can be inferred. Six frequently used U. S. AFGL reference atmospheres (McClatchey et al., 1972) are typical models which provide information on vertical thermodynamic structures and gaseous concentrations. These are commonly known as (1) Tropical, (2) Midlatitude Summer, (3) Midlatitude Winter, (4) Subarctic Summer, (5) Subarctic Winter, and (6) U. S. Standard Atmosphere models. Model atmospheres (1) to (6) all provide the vertical profiles of level pressure, temperature, absolute humidity, and ozone partial pressure from the sea level to the 100 km altitude (Kneizys et al., 1988).

Examining radiative properties of the East Asian atmosphere during the summer, it may be reasonable to use the Midlatitude Summer model atmosphere for the radiative transfer calculation because East Asia is located in the midlatitude band. However, because of the nature of varying atmospheric conditions with time and location, the use of over-simplified model atmospheres may give rise to uncertain outcomes, which may lead to less accurate interpretations. Therefore, more precise specification of atmospheric conditions is needed. In response to such a need, in particular for the East Asian region, we construct seasonally varying vertical profiles of thermodynamic variables over East

*E-mail: sohn@snu.ac.kr

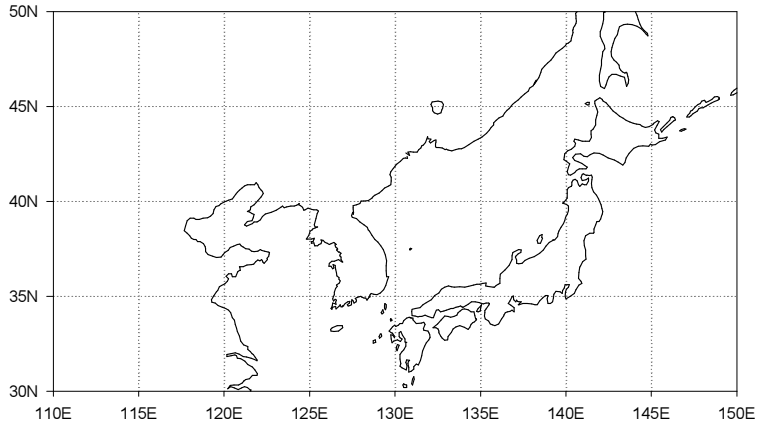

Fig. 1. Geographical map (30°–50°N, 110°–150°E) showing the East Asian domain used in this study.

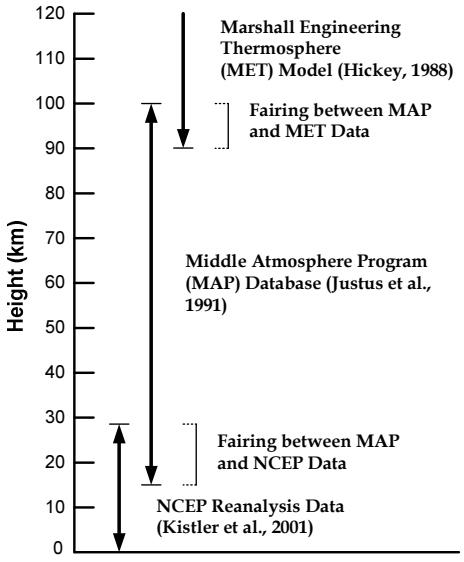

Fig. 2. Schematic summary of the atmospheric regions in the GRAM-95 program (Justus et al., 1995), and the sources for the models and data used in this study. Nomenclatures for the abbreviated forms are found in the text.

Asia, by synthesizing various observations and model output data. In addition, these newly constructed atmospheric data will then be used as basic inputs to examining the optical properties of the East Asian atmosphere.

2. Construction of the East Asian reference atmosphere

Various observations and model data are used for constructing the reference atmosphere over the East Asian domain (30°–50°N, 110°–150°E)— see Fig. 1. The method of synthesizing data from various sources is based on the National Aeronautics and Space Administration (NASA) Marshall Space Flight Center (MSFC) Global Reference Atmospheric Model (GRAM)—1995 Version (Justus et al., 1995). In this section, brief summaries of the data sets used and GRAM-95 synthesizing methods are introduced.

The main thermodynamic data in the lower altitude from zero to 27 km (surface–10 hPa pressure level) are obtained from monthly mean products of U. S. National Centers for Environmental Predictions (NCEP) reanalysis data (Kistler et al., 2001)— downloaded from National Oceanic and Atmospheric Administration (NOAA) Climate Diagnostic Centers (http://www.cdc.noaa.gov). NCEP water vapor information is used up to the 300 hPa level because of the availability of water vapor products. Mean temperature and moisture profiles over a 30-year period (1968–97) are thus produced for spring (March, April, and May), summer (June, July, and August), fall (September, October, and November), and winter (December, January, and February).

The atmospheric conditions in the stratosphere and middle atmosphere (20 to 100 km) are provided by a dataset compiled from Middle Atmosphere Program (MAP) data (Labitzke et al., 1985). In MAP data, the zonal monthly means of pressure, density, and temperature are gridded in 10 degree latitude and 5 km altitude increments. For the atmosphere above 90 km, simulation results by the Jacchia (1970) model, with an aid of the Marshall Engineering Thermosphere model (MET; Hickey, 1988), are employed. The MET model provides the species concentrations for N_2, O_2, O, Ar, He, and H above 90 km. The Jacchia model is designed to compute atmospheric density and temperature above 90 km using the species concentrations provided by the MET model.

The NCEP 30-year mean data provide water va-

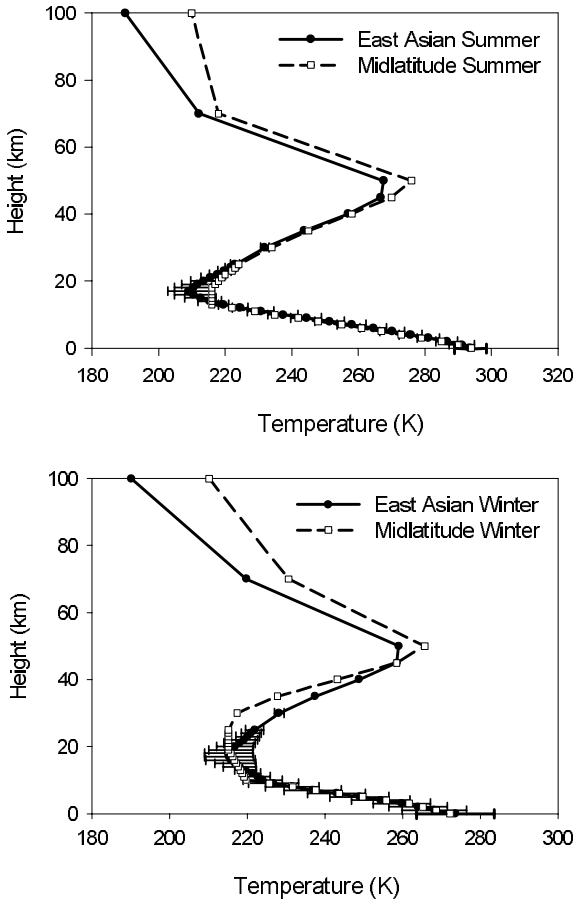

Fig. 3. Vertical profiles of temperature of the East Asia reference atmosphere and McClatchey et al. (1972) midlatitude atmosphere for the summer (top) and winter (bottom). Horizontal bars represent the standard errors for the seasonal mean.

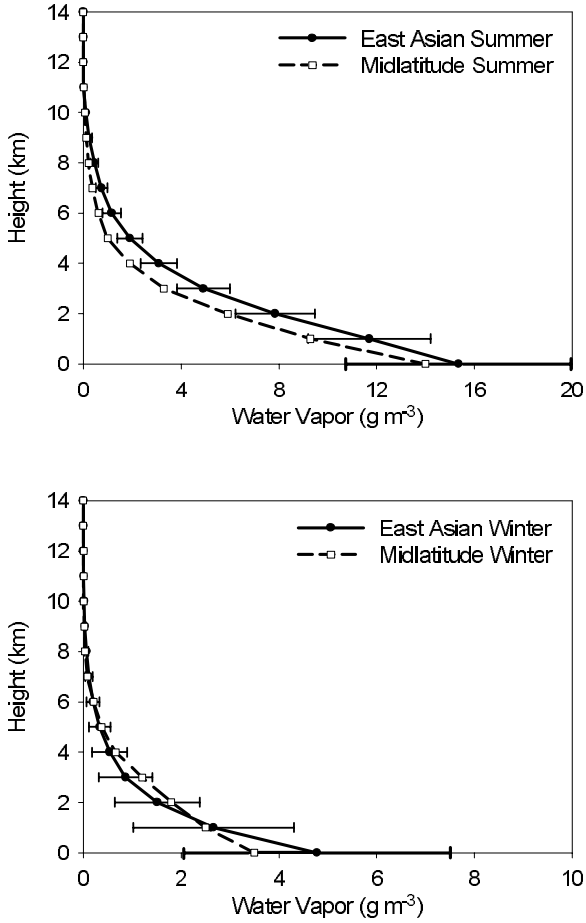

Fig. 4. Same as in Fig. 3 except for water vapor.

por profiles only up to 300 hPa level. Above the 300 hPa level GRAM-95 results are used. In the GRAM-95 model, for water vapor distributions, the NASA Langley Research Center (LaRC) water vapor climatology data are used (McCormick and Chiou, 1994) for altitudes up to 40.5 km; and above 40.5 km, MAP H_2O concentration data are used. For O_3 concentration, we employed results obtained from running the GRAM-95 model with data sets from the MET Jacchia model and AFGL atmospheric constituent profiles as inputs. Other trace gases (N_2O, CO, and CH_4) were also obtained by running the GRAM-95 model, but with MAP data for 20–120 km altitudes, and Jacchia model outputs for heights above 90 km.

Since there are overlapping altitude ranges between various thermodynamic data sets (e.g., 20 to 27 km for the GUACA and MAP data, and 90 to 120 km for the MAP and MET model outputs), we employ a fairing method used in GRAM-95 (Justus et al., 1995) in which the weighting for each dataset depends on the altitude of the overlapping range (Fig. 2). For example, a linearly varying weighting from zero to one, from the base to the top of the overlapping layer, can be applied to one dataset, while weighting from one to zero, from the top to the base, is applied to the other dataset. Thus, in the middle of the faring layer, the result is a simple arithmetic mean of values from two datasets. For the construction of a seasonally varying reference atmosphere we first take the domain average of temperature and humidity profiles for the given season and then a fairing technique is applied for smoothing. In this procedure, variability of temperature and moisture profiles is allowed only in the troposphere, as assured from the variance distributions of Figs. 3 and 4, which show much smaller variability above the tropopause.

An updated version (GRAM-99) is now available (Justus and Johnson, 1999) and thus can be used instead of GRAM-95. However, considering these two

Table 1. East Asian reference atmosphere (Spring).

Height (km)	Pressure (hPa)	T (K)	Density (g m^{-3})	H_2O (g m^{-3})	O_3 (g m^{-3})	N_2O (g m^{-3})	CO (g m^{-3})	CH_4 (g m^{-3})
0	1.016×10^{3}	281.7	1.251×10^{3}	7.170×10^{0}	6.884×10^{-5}	7.102×10^{-4}	2.293×10^{-4}	1.549×10^{-3}
1	8.994×10^{2}	278.6	1.123×10^{3}	4.720×10^{0}	6.565×10^{-5}	6.359×10^{-4}	1.986×10^{-4}	1.387×10^{-3}
2	7.953×10^{2}	274.3	1.009×10^{3}	2.967×10^{0}	6.257×10^{-5}	5.710×10^{-4}	1.721×10^{-4}	1.245×10^{-3}
3	7.016×10^{2}	269.1	9.075×10^{2}	1.831×10^{0}	6.245×10^{-5}	5.133×10^{-4}	1.494×10^{-4}	1.120×10^{-3}
4	6.174×10^{2}	263.3	8.164×10^{2}	1.166×10^{0}	6.180×10^{-5}	4.616×10^{-4}	1.302×10^{-4}	1.007×10^{-3}
5	5.416×10^{2}	257.5	7.326×10^{2}	7.314×10^{-1}	6.525×10^{-5}	4.141×10^{-4}	1.159×10^{-4}	8.994×10^{-4}
6	4.741×10^{2}	251.4	6.570×10^{2}	4.465×10^{-1}	6.797×10^{-5}	3.713×10^{-4}	1.032×10^{-4}	7.995×10^{-4}
7	4.132×10^{2}	244.6	5.884×10^{2}	2.677×10^{-1}	7.442×10^{-5}	3.324×10^{-4}	8.955×10^{-5}	7.091×10^{-4}
8	3.589×10^{2}	237.9	5.255×10^{2}	1.425×10^{-1}	7.984×10^{-5}	2.968×10^{-4}	7.607×10^{-5}	6.272×10^{-4}
9	3.104×10^{2}	231.2	4.676×10^{2}	7.002×10^{-2}	9.334×10^{-5}	2.616×10^{-4}	6.197×10^{-5}	5.544×10^{-4}
10	2.676×10^{2}	225.6	4.131×10^{2}	2.513×10^{-2}	1.080×10^{-4}	2.275×10^{-4}	4.997×10^{-5}	4.809×10^{-4}
11	2.298×10^{2}	221.8	3.608×10^{2}	5.965×10^{-3}	1.323×10^{-4}	1.926×10^{-4}	3.937×10^{-5}	4.113×10^{-4}
12	1.969×10^{2}	219.1	3.131×10^{2}	2.547×10^{-3}	1.528×10^{-4}	1.644×10^{-4}	2.977×10^{-5}	3.505×10^{-4}
13	1.685×10^{2}	217.6	2.700×10^{2}	1.251×10^{-3}	1.727×10^{-4}	1.383×10^{-4}	2.092×10^{-5}	2.971×10^{-4}
14	1.441×10^{2}	216.1	2.325×10^{2}	7.086×10^{-4}	1.804×10^{-4}	1.167×10^{-4}	1.422×10^{-5}	2.509×10^{-4}
15	1.231×10^{2}	214.9	1.997×10^{2}	4.897×10^{-4}	1.766×10^{-4}	9.752×10^{-5}	9.569×10^{-6}	2.116×10^{-4}
16	1.050×10^{2}	213.6	1.714×10^{2}	4.091×10^{-4}	1.820×10^{-4}	8.074×10^{-5}	6.393×10^{-6}	1.779×10^{-4}
17	8.956×10^{1}	213.2	1.465×10^{2}	3.679×10^{-4}	2.048×10^{-4}	6.458×10^{-5}	4.434×10^{-6}	1.487×10^{-4}
18	7.637×10^{1}	213.4	1.248×10^{2}	3.431×10^{-4}	2.526×10^{-4}	5.015×10^{-5}	2.990×10^{-6}	1.233×10^{-4}
19	6.509×10^{1}	213.9	1.061×10^{2}	3.188×10^{-4}	3.125×10^{-4}	3.712×10^{-5}	2.000×10^{-6}	1.017×10^{-4}
20	5.556×10^{1}	215.2	9.001×10^{1}	2.889×10^{-4}	3.521×10^{-4}	2.809×10^{-5}	1.455×10^{-6}	8.237×10^{-5}
21	4.741×10^{1}	216.5	7.631×10^{1}	2.599×10^{-4}	3.646×10^{-4}	2.030×10^{-5}	1.141×10^{-6}	6.614×10^{-5}
22	4.053×10^{1}	218.0	6.477×10^{1}	2.314×10^{-4}	3.686×10^{-4}	1.550×10^{-5}	9.686×10^{-7}	5.223×10^{-5}
23	3.466×10^{1}	219.4	5.506×10^{1}	2.040×10^{-4}	3.733×10^{-4}	1.213×10^{-5}	8.773×10^{-7}	4.070×10^{-5}
24	2.966×10^{1}	220.5	4.688×10^{1}	1.786×10^{-4}	3.687×10^{-4}	9.685×10^{-6}	7.983×10^{-7}	3.166×10^{-5}
25	2.540×10^{1}	221.4	3.998×10^{1}	1.555×10^{-4}	3.660×10^{-4}	7.661×10^{-6}	7.357×10^{-7}	2.455×10^{-5}
30	1.195×10^{1}	229.6	1.814×10^{1}	7.466×10^{-5}	2.251×10^{-4}	2.614×10^{-6}	4.169×10^{-7}	1.060×10^{-5}
35	5.841×10^{0}	243.4	8.363×10^{0}	3.580×10^{-5}	1.141×10^{-4}	6.114×10^{-7}	2.344×10^{-7}	3.537×10^{-6}
40	2.980×10^{0}	257.6	4.029×10^{0}	1.513×10^{-5}	4.412×10^{-5}	1.140×10^{-7}	1.351×10^{-7}	1.255×10^{-6}
45	1.573×10^{0}	267.7	2.047×10^{0}	6.717×10^{-6}	1.390×10^{-5}	2.821×10^{-8}	8.425×10^{-8}	4.840×10^{-7}
50	8.423×10^{-1}	267.8	1.095×10^{0}	3.603×10^{-6}	4.596×10^{-6}	7.893×10^{-9}	6.681×10^{-8}	1.970×10^{-7}
70	5.389×10^{-2}	220.6	8.514×10^{-2}	1.829×10^{-7}	4.055×10^{-8}	1.421×10^{-10}	4.754×10^{-8}	9.263×10^{-9}
100	3.021×10^{-4}	189.2	5.440×10^{-4}	1.515×10^{-10}	3.937×10^{-10}	3.012×10^{-13}	9.736×10^{-9}	4.839×10^{-11}

Note: T means temperature, the same hereafter.

versions are nearly the same, except for updated MAP data and the MET model used for GRAM-95, differences in results drawn from the two versions are thought to be insignificant.

3. East Asian reference atmosphere

The resultant atmospheric conditions over East Asia (whose domain is given in Fig. 1) for the spring, summer, fall, and winter are presented in Tables 1 to 4, respectively—these are referred to as the East Asia (EA) reference atmospheres. In these tables, pressure, density of air, and H_2O, O_3, N_2O, CO, and CH_4 concentrations are provided at the given altitude.

In order to highlight the atmospheric profile representing East Asia, the EA summer and winter atmospheres are compared with McClatchey et al. (1972) midlatitude summer (MS) and winter (MW) temperature profiles, water vapor, and ozone concentrations. Plots are given in Figs. 3–5, respectively. To show the degree to which the variability of thermodynamic structures in the lower troposphere is due to their spatial and temporal variations, error bars are provided at each altitude using one standard deviation averaged over the domain.

In Fig. 3, temperature profiles for East Asia as a function of altitude are shown for up to 100 km, together with those from MS and MW of McClatchey et al. (1972). During the summer it is noted that the EA reference atmosphere shows a general agreement between the temperature profiles with MS in the lower troposphere below around 15 km. The largest differences, however, are found in the tropopause layer where the EA atmosphere shows colder conditions during the summer. The largest variability is noted in the tropopause level centered at around 18 km altitude. Temperature variability appears to be larger during the winter. Noticeable differences are found above 40 km. On the other hand, significant differences in temperature are found during the winter above the tropopause level, although similar profiles are shown in the tropospheric layer.

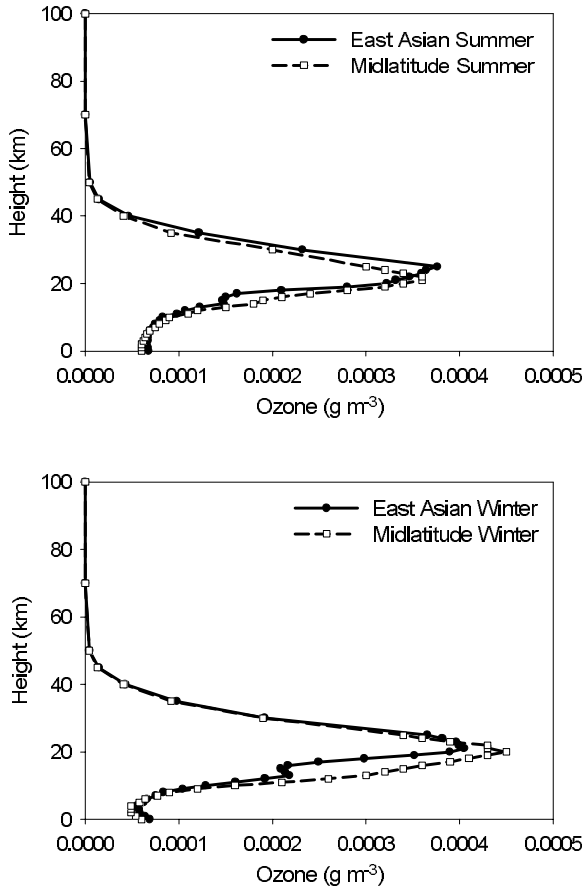

Fig. 5. Same as in Fig. 3 except for ozone.

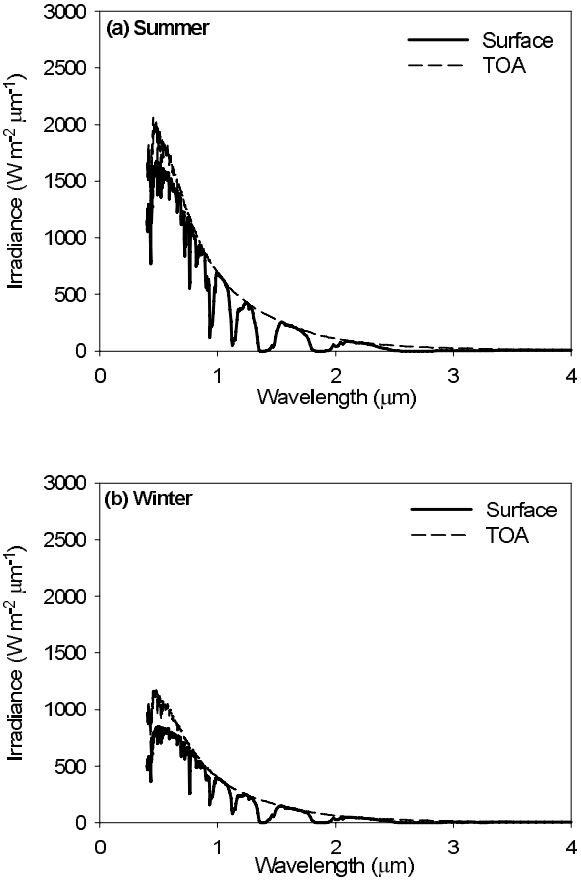

Fig. 6. Solar irradiance distributions at the TOA and at the surface for a solar zenith angle of (a) 18° in an EA summer atmosphere and (b) 57° in an EA winter atmosphere without aerosols or clouds.

In contrast, significantly different vertical distributions of water vapor concentration are noted in summer (Fig. 4). During the summer, the EA reference atmosphere is moister throughout the atmospheric layer than the MS model atmosphere, reflecting the presence of hot and humid air associated with the northwestward expansion of the North Pacific High pressure system during the summer over most of East Asia, in response to the progress of the Asian monsoon system. Total precipitable waters (TPWs) for the EA summer and MS atmospheres are 40.6 kg m^{-2} and 30.2 kg m^{-2}, respectively. On the other hand, the comparison for the winter shows that the boundary layer is moister and the middle tropospheric layer is drier, probably influenced by the Siberian High but modified by moist oceanic conditions within the shallow boundary layer in the southeast region of the East Asian domain. TPW of 8.8 kg m^{-2} is noted for both EA winter and MW atmospheres. Water vapor variability shows the maximum at the surface level (11 to 20 g m^{-3} for the summer, and 2 to 7.5 g m^{-3} for the winter) and decreases with height and reaches near zero around 11 km altitude. Summertime shows relatively larger variability compared with the winter. As shown in the water vapor variability with season and geographical location, care must be taken when water vapor profiles of the midlatitude reference atmosphere of McClatchey et al. (1972) are used as inputs to the radiative transfer calculation over East Asia, particularly when water vapor absorption is under consideration.

Ozone concentrations (Fig. 5) of the EA reference atmosphere are not much different from McClatchey et al. (1972) except for the lower stratosphere during the winter, where the EA reference atmosphere shows a much smaller ozone concentration.

4. Optical properties of the East Asian reference atmosphere

In order to examine the mean optical properties of the atmosphere over East Asia we calculated downwelling solar irradiance at the top of the atmosphere

Table 2. East Asian reference atmosphere (Summer).

Height (km)	Pressure (hPa)	T (K)	Density (g m^{-3})	H_2O (g m^{-3})	O_3 (g m^{-3})	N_2O (g m^{-3})	CO (g m^{-3})	CH_4 (g m^{-3})
0	1.009×10^{3}	293.6	1.188×10^{3}	1.535×10^{1}	6.775×10^{-5}	6.766×10^{-4}	2.186×10^{-4}	1.476×10^{-3}
1	8.986×10^{2}	291.1	1.069×10^{3}	1.170×10^{1}	6.701×10^{-5}	6.076×10^{-4}	1.898×10^{-4}	1.326×10^{-3}
2	7.988×10^{2}	286.6	9.663×10^{2}	7.848×10^{0}	6.602×10^{-5}	5.485×10^{-4}	1.654×10^{-4}	1.197×10^{-3}
3	7.086×10^{2}	281.1	8.750×10^{2}	4.913×10^{0}	6.669×10^{-5}	4.960×10^{-4}	1.444×10^{-4}	1.082×10^{-3}
4	6.273×10^{2}	275.7	7.908×10^{2}	3.090×10^{0}	6.678×10^{-5}	4.478×10^{-4}	1.263×10^{-4}	9.772×10^{-4}
5	5.537×10^{2}	270.2	7.128×10^{2}	1.907×10^{0}	6.738×10^{-5}	4.033×10^{-4}	1.129×10^{-4}	8.762×10^{-4}
6	4.878×10^{2}	264.5	6.417×10^{2}	1.168×10^{0}	6.891×10^{-5}	3.628×10^{-4}	1.008×10^{-4}	7.817×10^{-4}
7	4.281×10^{2}	258.0	5.776×10^{2}	7.483×10^{-1}	7.265×10^{-5}	3.264×10^{-4}	8.796×10^{-5}	6.965×10^{-4}
8	3.747×10^{2}	251.4	5.191×10^{2}	4.448×10^{-1}	7.479×10^{-5}	2.933×10^{-4}	7.519×10^{-5}	6.198×10^{-4}
9	3.266×10^{2}	244.4	4.655×10^{2}	2.402×10^{-1}	8.011×10^{-5}	2.603×10^{-4}	6.170×10^{-5}	5.520×10^{-4}
10	2.839×10^{2}	237.4	4.164×10^{2}	1.004×10^{-1}	8.297×10^{-5}	2.291×10^{-4}	5.036×10^{-5}	4.847×10^{-4}
11	2.455×10^{2}	230.7	3.706×10^{2}	1.704×10^{-2}	9.831×10^{-5}	1.977×10^{-4}	4.043×10^{-5}	4.225×10^{-4}
12	2.114×10^{2}	224.5	3.280×10^{2}	7.072×10^{-3}	1.069×10^{-4}	1.722×10^{-4}	3.119×10^{-5}	3.672×10^{-4}
13	1.814×10^{2}	219.6	2.878×10^{2}	3.132×10^{-3}	1.226×10^{-4}	1.475×10^{-4}	2.231×10^{-5}	3.169×10^{-4}
14	1.552×10^{2}	215.4	2.510×10^{2}	1.510×10^{-3}	1.482×10^{-4}	1.260×10^{-4}	1.536×10^{-5}	2.710×10^{-4}
15	1.324×10^{2}	212.6	2.170×10^{2}	8.573×10^{-4}	1.467×10^{-4}	1.060×10^{-4}	1.040×10^{-5}	2.300×10^{-4}
16	1.128×10^{2}	210.4	1.868×10^{2}	5.772×10^{-4}	1.500×10^{-4}	8.797×10^{-5}	6.968×10^{-6}	1.939×10^{-4}
17	9.574×10^{1}	209.1	1.596×10^{2}	4.411×10^{-4}	1.620×10^{-4}	7.036×10^{-5}	4.833×10^{-6}	1.621×10^{-4}
18	8.142×10^{1}	210.4	1.349×10^{2}	3.686×10^{-4}	2.097×10^{-4}	5.421×10^{-5}	3.232×10^{-6}	1.333×10^{-4}
19	6.928×10^{1}	211.8	1.140×10^{2}	3.239×10^{-4}	2.797×10^{-4}	3.992×10^{-5}	2.151×10^{-6}	1.093×10^{-4}
20	5.906×10^{1}	213.6	9.632×10^{1}	2.879×10^{-4}	3.220×10^{-4}	3.000×10^{-5}	1.558×10^{-6}	8.817×10^{-5}
21	5.037×10^{1}	215.6	8.140×10^{1}	2.572×10^{-4}	3.318×10^{-4}	2.143×10^{-5}	1.218×10^{-6}	7.057×10^{-5}
22	4.296×10^{1}	217.7	6.874×10^{1}	2.284×10^{-4}	3.462×10^{-4}	1.605×10^{-5}	1.028×10^{-6}	5.545×10^{-5}
23	3.672×10^{1}	219.8	5.820×10^{1}	2.019×10^{-4}	3.591×10^{-4}	1.249×10^{-5}	9.277×10^{-7}	4.304×10^{-5}
24	3.142×10^{1}	221.6	4.940×10^{1}	1.779×10^{-4}	3.646×10^{-4}	9.872×10^{-6}	8.416×10^{-7}	3.337×10^{-5}
25	2.693×10^{1}	223.0	4.205×10^{1}	1.561×10^{-4}	3.763×10^{-4}	7.833×10^{-6}	7.776×10^{-7}	2.579×10^{-5}
30	1.276×10^{1}	231.9	1.916×10^{1}	7.675×10^{-5}	2.321×10^{-4}	3.157×10^{-6}	4.661×10^{-7}	1.109×10^{-5}
35	6.259×10^{0}	243.7	8.945×10^{0}	3.796×10^{-5}	1.217×10^{-4}	7.437×10^{-7}	2.708×10^{-7}	4.117×10^{-6}
40	3.192×10^{0}	256.9	4.329×10^{0}	1.647×10^{-5}	4.637×10^{-5}	1.288×10^{-7}	1.574×10^{-7}	1.403×10^{-6}
45	1.682×10^{0}	266.8	2.196×10^{0}	7.615×10^{-6}	1.485×10^{-5}	3.359×10^{-8}	9.228×10^{-8}	5.565×10^{-7}
50	8.989×10^{-1}	267.6	1.171×10^{0}	3.797×10^{-6}	5.124×10^{-6}	9.797×10^{-9}	5.614×10^{-8}	2.307×10^{-7}
70	5.611×10^{-2}	212.2	9.210×10^{-2}	2.027×10^{-7}	4.301×10^{-8}	1.386×10^{-10}	1.474×10^{-8}	1.002×10^{-8}
100	2.819×10^{-4}	190.0	5.066×10^{-4}	1.408×10^{-10}	3.658×10^{-10}	2.689×10^{-13}	7.214×10^{-9}	4.497×10^{-11}

(TOA) and at the Earth's surface for the visible spectrum, and outgoing TOA radiance for infrared spectrums using the MODTRAN 4 radiative transfer model (Anderson et al., 2000; Berk et al., 1999) developed at the U. S. AFGL. For the radiance calculation, the constructed EA reference atmosphere is used for the input data.

Figure 6 shows solar irradiance at the top of the clear atmosphere (top dashed curve) and at the surface (bottom solid curve). Thus the difference between the two curves represents depletion of solar radiation due to the atmosphere. For the calculation, we used seasonal mean solar zenith angles (18.1° for the summer and 56.6° for the winter) for Seoul, Korea (37.34°N, 126.34°E), with a solar constant of 1368 W m^{-2}. The depletion of solar flux in the Earth's atmosphere is evident in the UV region (shorter than 0.4 μm) due to absorption by oxygen and ozone molecules. In the visible spectrum the depletion is mainly due to Rayleigh scattering, absorption by oxygen, ozone, and weak water vapor absorption (Liou, 2002). In the near infrared spectrum depletions are clear, in association with water vapor absorption. Also noted is absorption due to carbon dioxide in the 2.7 μm band.

It is well known that water vapor is the major absorbing gas in the near infrared spectrum, whose contribution to solar energy is around 50% (Goody and Young, 1989), suggesting that precise specification of water vapor profiles is a prerequisite for accurate calculation of solar fluxes. Since the East Asia reference atmospheres improve the accuracy of atmospheric conditions over East Asia, the use of EA water vapor profiles implies significant changes in calculated solar irradiances in comparison to those from MS and MW atmospheres. In order to examine the impact of improved atmospheric profiles on the solar fluxes, differences in surface solar irradiance between from EA reference atmospheres and from McClatchey et al. (1972) midlatitude models (MS, MW) are obtained in the solar spectrum range (Fig. 7).

During the summer the use of EA reference atmospheres resulted in significant reduction of solar irradiance at the surface over the spectra centered at 0.72, 0.82, 0.94, 1.1, 1.38, and 1.87 μm due to the higher water vapor absorption of the EA summer atmosphere. Total solar flux arriving at the surface (Fig. 6a) during

Table 3. East Asian reference atmosphere (Fall).

Height (km)	Pressure (hPa)	T (K)	Density (g m^{-3})	H_2O (g m^{-3})	O_3 (g m^{-3})	N_2O (g m^{-3})	CO (g m^{-3})	CH_4 (g m^{-3})
0	1.019×10^{3}	286.9	1.232×10^{3}	1.035×10^{1}	6.778×10^{-5}	6.993×10^{-4}	2.258×10^{-4}	1.525×10^{-3}
1	9.032×10^{2}	282.0	1.112×10^{3}	6.490×10^{0}	6.511×10^{-5}	6.306×10^{-4}	1.969×10^{-4}	1.376×10^{-3}
2	7.995×10^{2}	277.3	1.002×10^{3}	3.917×10^{0}	6.221×10^{-5}	5.677×10^{-4}	1.711×10^{-4}	1.239×10^{-3}
3	7.063×10^{2}	272.6	9.015×10^{2}	2.350×10^{0}	6.206×10^{-5}	5.101×10^{-4}	1.484×10^{-4}	1.113×10^{-3}
4	6.227×10^{2}	267.1	8.118×10^{2}	1.492×10^{0}	6.147×10^{-5}	4.592×10^{-4}	1.295×10^{-4}	1.002×10^{-3}
5	5.473×10^{2}	261.3	7.293×10^{2}	9.396×10^{-1}	6.497×10^{-5}	4.123×10^{-4}	1.154×10^{-4}	8.955×10^{-4}
6	4.801×10^{2}	255.4	6.547×10^{2}	5.838×10^{-1}	6.774×10^{-5}	3.701×10^{-4}	1.028×10^{-4}	7.969×10^{-4}
7	4.194×10^{2}	248.7	5.874×10^{2}	3.610×10^{-1}	7.429×10^{-5}	3.319×10^{-4}	8.940×10^{-5}	7.079×10^{-4}
8	3.652×10^{2}	242.2	5.251×10^{2}	2.061×10^{-1}	7.979×10^{-5}	2.967×10^{-4}	7.603×10^{-5}	6.268×10^{-4}
9	3.167×10^{2}	235.7	4.679×10^{2}	1.089×10^{-1}	9.340×10^{-5}	2.617×10^{-4}	6.201×10^{-5}	5.547×10^{-4}
10	2.738×10^{2}	230.1	4.144×10^{2}	4.521×10^{-2}	1.084×10^{-4}	2.281×10^{-4}	5.011×10^{-5}	4.824×10^{-4}
11	2.358×10^{2}	225.5	3.640×10^{2}	9.496×10^{-3}	1.335×10^{-4}	1.944×10^{-4}	3.972×10^{-5}	4.150×10^{-4}
12	2.025×10^{2}	221.5	3.183×10^{2}	4.197×10^{-3}	1.554×10^{-4}	1.672×10^{-4}	3.027×10^{-5}	3.564×10^{-4}
13	1.735×10^{2}	218.2	2.770×10^{2}	2.033×10^{-3}	1.772×10^{-4}	1.420×10^{-4}	2.147×10^{-5}	3.049×10^{-4}
14	1.483×10^{2}	215.1	2.404×10^{2}	1.100×10^{-3}	1.865×10^{-4}	1.207×10^{-4}	1.470×10^{-5}	2.594×10^{-4}
15	1.266×10^{2}	213.1	2.072×10^{2}	7.088×10^{-4}	1.831×10^{-4}	1.012×10^{-4}	9.925×10^{-6}	2.195×10^{-4}
16	1.078×10^{2}	211.3	1.781×10^{2}	5.389×10^{-4}	1.889×10^{-4}	8.385×10^{-5}	6.639×10^{-6}	1.847×10^{-4}
17	9.168×10^{1}	210.7	1.518×10^{2}	4.411×10^{-4}	2.120×10^{-4}	6.689×10^{-5}	4.592×10^{-6}	1.540×10^{-4}
18	7.805×10^{1}	211.8	1.285×10^{2}	3.727×10^{-4}	2.600×10^{-4}	5.164×10^{-5}	3.078×10^{-6}	1.270×10^{-4}
19	6.649×10^{1}	213.0	1.089×10^{2}	3.217×10^{-4}	3.206×10^{-4}	3.810×10^{-5}	2.053×10^{-6}	1.044×10^{-4}
20	5.672×10^{1}	214.3	9.225×10^{1}	2.826×10^{-4}	3.608×10^{-4}	2.879×10^{-5}	1.491×10^{-6}	8.442×10^{-5}
21	4.836×10^{1}	215.7	7.812×10^{1}	2.500×10^{-4}	3.731×10^{-4}	2.078×10^{-5}	1.168×10^{-6}	6.771×10^{-5}
22	4.129×10^{1}	217.3	6.621×10^{1}	2.214×10^{-4}	3.767×10^{-4}	1.585×10^{-5}	9.902×10^{-7}	5.340×10^{-5}
23	3.526×10^{1}	218.7	5.618×10^{1}	1.959×10^{-4}	3.809×10^{-4}	1.238×10^{-5}	8.953×10^{-7}	4.154×10^{-5}
24	3.014×10^{1}	219.9	4.776×10^{1}	1.728×10^{-4}	3.756×10^{-4}	9.867×10^{-6}	8.134×10^{-7}	3.226×10^{-5}
25	2.578×10^{1}	220.8	4.068×10^{1}	1.518×10^{-4}	3.723×10^{-4}	7.794×10^{-6}	7.485×10^{-7}	2.498×10^{-5}
30	1.206×10^{1}	227.4	1.850×10^{1}	7.374×10^{-5}	2.105×10^{-4}	3.476×10^{-6}	4.249×10^{-7}	1.161×10^{-5}
35	5.831×10^{0}	237.5	8.558×10^{0}	3.550×10^{-5}	1.095×10^{-4}	7.531×10^{-7}	2.398×10^{-7}	4.132×10^{-6}
40	2.918×10^{0}	249.7	4.073×10^{0}	1.505×10^{-5}	4.514×10^{-5}	1.317×10^{-7}	1.365×10^{-7}	1.470×10^{-6}
45	1.509×10^{0}	260.4	2.019×10^{0}	6.739×10^{-6}	1.509×10^{-5}	3.255×10^{-8}	8.309×10^{-8}	5.862×10^{-7}
50	7.965×10^{-1}	262.7	1.056×10^{0}	3.515×10^{-6}	4.510×10^{-6}	9.809×10^{-9}	6.437×10^{-8}	2.570×10^{-7}
70	4.849×10^{-2}	218.0	7.750×10^{-2}	1.541×10^{-7}	3.073×10^{-8}	1.293×10^{-10}	4.343×10^{-8}	8.429×10^{-9}
100	3.213×10^{-4}	188.0	5.823×10^{-4}	1.621×10^{-10}	4.214×10^{-10}	3.224×10^{-13}	1.043×10^{-8}	5.179×10^{-11}

the summer is 894.6 W m^{-2} for the EA atmosphere, compared with 908.9 W m^{-2} from the MS atmosphere, resulting in a 14.3 W m^{-2} difference. However, the EA winter atmosphere (Fig. 7b) shows indiscernible difference. Solar fluxes reaching the surface during the winter are 513.1 W m^{-2} and 513.6 W m^{-2} for EA winter and MW atmospheres, respectively, resulting in a small difference of 0.5 W m^{-2}. From this comparison, it is concluded that water vapor distribution during the summer may be the major cause of uncertainties in the radiative transfer calculation over the East Asian study region when McClatchey et al. (1972) model atmospheres are used.

Also provided in Fig. 7 are irradiance ranges induced by moisture profiles departed with one standard deviation from the mean profile (i.e., $\pm\sigma_q$) in Fig. 4. In this calculation, temperature profiles are fixed with the mean profile. It is shown that water vapor variability can give irradiance variability as large as the difference between EA and ML atmospheres. Similar magnitudes of irradiance variability are found for the winter, although the difference between EA and ML is indiscernible. Again, results emphasize that specification of accurate water vapor distribution is a prerequisite for radiative transfer calculation over the East Asian study region.

The spectral distribution of radiant energy emitted from the East Asian earth–atmosphere system is given in terms of wave number (Fig. 8). Also provided are spectral distributions of radiance emitted by blackbody sources of surface temperature 300 K, 275 K (dashed curves in Fig. 8). It is clearly shown that certain portions of the infrared radiation spectrum are trapped by the atmospheric gases, e.g. absorption by carbon dioxide in the 15 μm band from 600 to 800 cm^{-1}, where the maximum intensity of the Planck function is located; water vapor absorption in the 6.3 μm band from around 1200 to 2000 cm^{-1} and in the spectral region of less than 500 cm^{-1}; and ozone absorption in the 9.7 μm band around 1000 cm^{-1}.

Since the EA reference atmospheres differ from the McClatchey et al. (1972) midlatitude atmospheres, particularly in the water vapor and ozone profiles, the strong infrared absorption by water vapor and ozone implies that there must exist significant radiance differences between the two model atmospheres in com-

Table 4. East Asian reference atmosphere (Winter).

Height (km)	Pressure (hPa)	T (K)	Density (g m^{-3})	H_2O (g m^{-3})	O_3 (g m^{-3})	N_2O (g m^{-3})	CO (g m^{-3})	CH_4 (g m^{-3})
0	1.023×10^{3}	273.6	1.300×10^{3}	4.783×10^{0}	6.899×10^{-5}	7.355×10^{-4}	2.375×10^{-4}	1.604×10^{-3}
1	9.006×10^{2}	268.2	1.169×10^{3}	2.669×10^{0}	6.361×10^{-5}	6.611×10^{-4}	2.065×10^{-4}	1.442×10^{-3}
2	7.922×10^{2}	264.0	1.045×10^{3}	1.513×10^{0}	5.828×10^{-5}	5.909×10^{-4}	1.781×10^{-4}	1.289×10^{-3}
3	6.956×10^{2}	259.8	9.324×10^{2}	8.659×10^{-1}	5.727×10^{-5}	5.270×10^{-4}	1.533×10^{-4}	1.149×10^{-3}
4	6.092×10^{2}	254.4	8.343×10^{2}	5.405×10^{-1}	5.580×10^{-5}	4.715×10^{-4}	1.330×10^{-4}	1.029×10^{-3}
5	5.320×10^{2}	248.9	7.447×10^{2}	3.364×10^{-1}	6.226×10^{-5}	4.208×10^{-4}	1.178×10^{-4}	9.139×10^{-4}
6	4.636×10^{2}	243.0	6.646×10^{2}	2.019×10^{-1}	6.615×10^{-5}	3.756×10^{-4}	1.043×10^{-4}	8.086×10^{-4}
7	4.022×10^{2}	236.8	5.917×10^{2}	1.161×10^{-1}	7.528×10^{-5}	3.344×10^{-4}	9.005×10^{-5}	7.130×10^{-4}
8	3.478×10^{2}	231.6	5.231×10^{2}	6.256×10^{-2}	8.351×10^{-5}	2.957×10^{-4}	7.574×10^{-5}	6.244×10^{-4}
9	2.997×10^{2}	226.8	4.602×10^{2}	3.389×10^{-2}	1.042×10^{-4}	2.576×10^{-4}	6.099×10^{-5}	5.456×10^{-4}
10	2.578×10^{2}	224.0	4.007×10^{2}	1.499×10^{-2}	1.288×10^{-4}	2.207×10^{-4}	4.846×10^{-5}	4.664×10^{-4}
11	2.213×10^{2}	222.7	3.461×10^{2}	4.907×10^{-3}	1.607×10^{-4}	1.848×10^{-4}	3.776×10^{-5}	3.946×10^{-4}
12	1.899×10^{2}	221.3	2.990×10^{2}	2.162×10^{-3}	1.921×10^{-4}	1.571×10^{-4}	2.842×10^{-5}	3.347×10^{-4}
13	1.628×10^{2}	219.6	2.583×10^{2}	1.087×10^{-3}	2.181×10^{-4}	1.324×10^{-4}	2.001×10^{-5}	2.842×10^{-4}
14	1.394×10^{2}	218.0	2.231×10^{2}	6.350×10^{-4}	2.135×10^{-4}	1.120×10^{-4}	1.364×10^{-5}	2.407×10^{-4}
15	1.192×10^{2}	216.9	1.918×10^{2}	4.567×10^{-4}	2.087×10^{-4}	9.369×10^{-5}	9.186×10^{-6}	2.031×10^{-4}
16	1.019×10^{2}	215.7	1.648×10^{2}	3.910×10^{-4}	2.167×10^{-4}	7.765×10^{-5}	6.144×10^{-6}	1.710×10^{-4}
17	8.699×10^{1}	215.3	1.410×10^{2}	3.554×10^{-4}	2.495×10^{-4}	6.214×10^{-5}	4.265×10^{-6}	1.430×10^{-4}
18	7.428×10^{1}	215.2	1.204×10^{2}	3.314×10^{-4}	2.984×10^{-4}	4.837×10^{-5}	2.883×10^{-6}	1.189×10^{-4}
19	6.340×10^{1}	215.8	1.025×10^{2}	3.052×10^{-4}	3.516×10^{-4}	3.585×10^{-5}	1.931×10^{-6}	9.818×10^{-5}
20	5.419×10^{1}	216.9	8.711×10^{1}	2.745×10^{-4}	3.896×10^{-4}	2.726×10^{-5}	1.408×10^{-6}	7.969×10^{-5}
21	4.633×10^{1}	218.0	7.407×10^{1}	2.466×10^{-4}	4.050×10^{-4}	1.993×10^{-5}	1.107×10^{-6}	6.419×10^{-5}
22	3.963×10^{1}	219.1	6.304×10^{1}	2.204×10^{-4}	3.991×10^{-4}	1.547×10^{-5}	9.426×10^{-7}	5.083×10^{-5}
23	3.390×10^{1}	220.1	5.368×10^{1}	1.957×10^{-4}	3.965×10^{-4}	1.216×10^{-5}	8.553×10^{-7}	3.968×10^{-5}
24	2.899×10^{1}	221.0	4.571×10^{1}	1.722×10^{-4}	3.816×10^{-4}	9.748×10^{-6}	7.785×10^{-7}	3.087×10^{-5}
25	2.484×10^{1}	221.9	3.901×10^{1}	1.503×10^{-4}	3.654×10^{-4}	7.696×10^{-6}	7.138×10^{-7}	2.402×10^{-5}
30	1.169×10^{1}	228.2	1.784×10^{1}	7.179×10^{-5}	1.916×10^{-4}	2.954×10^{-6}	3.856×10^{-7}	1.117×10^{-5}
35	5.652×10^{0}	237.5	8.295×10^{0}	3.595×10^{-5}	9.801×10^{-5}	5.477×10^{-7}	2.131×10^{-7}	3.566×10^{-6}
40	2.823×10^{0}	248.8	3.956×10^{0}	1.475×10^{-5}	4.275×10^{-5}	8.174×10^{-8}	1.208×10^{-7}	1.146×10^{-6}
45	1.456×10^{0}	258.5	1.963×10^{0}	6.034×10^{-6}	1.477×10^{-5}	1.842×10^{-8}	7.870×10^{-8}	4.229×10^{-7}
50	7.636×10^{-1}	259.0	1.027×10^{0}	3.449×10^{-6}	4.426×10^{-6}	5.469×10^{-9}	7.548×10^{-8}	1.760×10^{-7}
70	4.501×10^{-2}	219.7	7.139×10^{-2}	1.322×10^{-7}	3.244×10^{-8}	1.311×10^{-10}	6.557×10^{-8}	7.762×10^{-9}
100	3.379×10^{-4}	190.1	6.057×10^{-4}	1.686×10^{-10}	4.381×10^{-10}	3.478×10^{-13}	1.288×10^{-8}	5.385×10^{-11}

parison. In order to examine what degree of spectral radiant intensity, and thus flux, is changed in association with the replacement by an EA reference atmosphere, differences are taken by subtracting radiance from the McClatchey et al. (1972) atmosphere (Fig. 9). Also delineated are radiance differences between the EA profile with one standard deviation and the McClatchey et al. (1972) atmosphere for examining the effect of variability in the EA atmosphere on the spectral radiance.

For the summer (Fig. 9a) it is noted that emitted infrared radiances are significantly reduced for the East Asian atmosphere compared with infrared emissions for the MS atmosphere. Total emitted fluxes at the TOA for the EA summer and MS atmospheres are 274.5 W m^{-2} and 281.0 W m^{-2}, respectively, which would result in a 6.5 W m^{-2} reduction of the emitted radiation when the EA summer atmosphere is used. Such a reduction is clearly due to the increase of water vapor absorption by the EA atmosphere, in a wavelength range less than 500 cm^{-1}, and from 1200 to 2000 cm^{-1}. Reduced radiances due to the increased ozone absorption by the EA atmosphere are also noted over the atmospheric window region from 800 to 1200 cm^{-1}. Radiant flux range due to the $\pm\sigma_q$ changes of effect indicates that the drier extreme of the moisture profile gives rise to spectral fluxes similar to those for the MS atmosphere. By the same token the wetter extreme brings in more reduction of the emitted radiation.

By contrast, the use of the EA reference atmosphere for the winter in place of the MW atmosphere shows generally increased radiances over the carbon dioxide, ozone absorption bands. It appears that increased radiances are due to the higher temperature of the EA atmosphere in the layer between 10 km and 40 km. However, a total flux difference of 2 W m^{-2} during the winter appears to be minor, considering that TOA fluxes for EA winter and MW are 228.9 W m^{-2} and 226.9 W m^{-2}, respectively. Examination of the effect $\pm\sigma_q$ changes have on radiance indicates that flux range is larger particularly over the water vapor rotational band between 14 μm and 40 μm, probably due to the large difference in the surface boundary layer moisture for the wetter EA atmosphere, in comparison to the McClatchey et al. (1972) atmosphere.

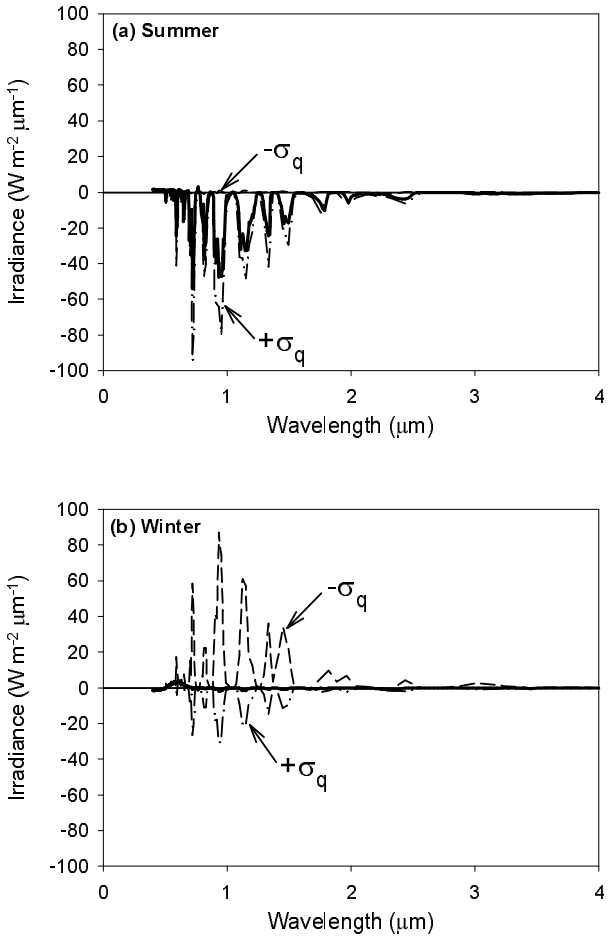

Fig. 7. Spectral distributions of solar irradiance difference between EA reference atmosphere and McClatchey et al. (1972) midlatitude (a) summer atmospheres and (b) winter atmospheres. Ranges enveloped by $+\sigma_q$ and $-\sigma_q$ curves represent irradiance variability due to the water vapor variability given in Fig. 4.

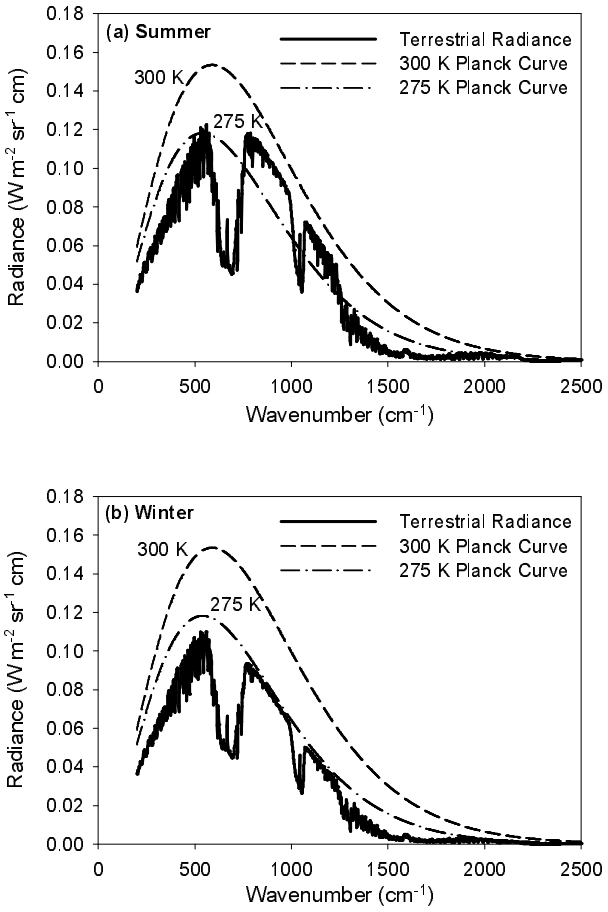

Fig. 8. Thermal infrared emission spectrum for the East Asia (a) summer and (b) winter atmospheres calculated using MODTRAN 4. Theoretical Planck radiance curves for 300 K, 275 K blackbody are also plotted.

5. Conclusions

Seasonally varying climatological reference atmospheres for the East Asia region (30°–50°N, 110°–150°E) are constructed using various observations, model outputs of atmospheric thermodynamic parameters and gaseous concentrations, with the aid of the GRAM-95 model (Justus et al., 1995). They were referred to as East Asia spring, summer, fall, and winter reference atmospheres.

The obtained East Asia summer and winter reference atmospheres were compared with midlatitude summer and winter atmospheres reported by McClatchey et al. (1972). A comparison of results indicates that major differences are shown in the water vapor field in particular during the summer, in which TPW for the EA summer is 40.6 kg m^{-2}, while for the McClatchey et al. (1972) midlatitude summer, it is 30.2 kg m^{-2}. However, nearly the same TPWs are found from the comparison for winter. Differences in temperature and ozone concentration between the two atmospheres appear comparatively smaller. It is noted that the use of the EA atmosphere during the summer resulted in more atmospheric absorption of solar radiation by as much as 14.3 W m^{-2}, and around 6.5 W m^{-2} more absorption of infrared radiation. Respective differences during the winter were 0.5 and 2 W m^{-2}. The relatively larger impact on thermal infrared radiation is likely to be associated with the temperature effect combined with carbon dioxide and ozone concentration.

In conclusion, the constructed seasonally varying reference atmospheres, designed for better specification of atmospheric conditions over the East Asian region, will bring in a better understanding of optical characteristics in East Asia, which will then be used to study various climate or remote sensing problems.

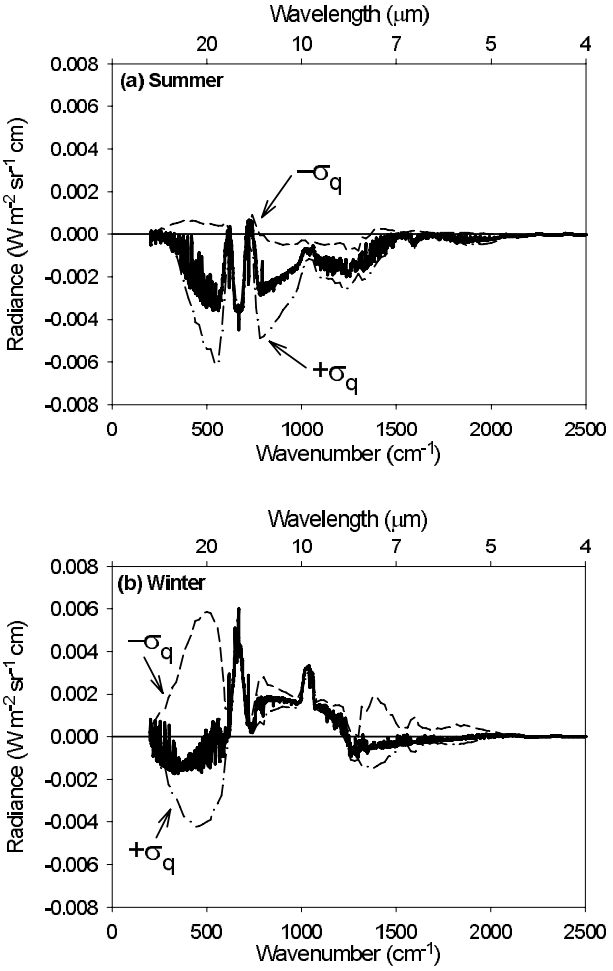

Fig. 9. Spectral distributions of thermal emission difference between the EA reference atmosphere and McClatchey et al. (1972) midlatitude (a) summer atmospheres and (b) winter atmospheres. Ranges enveloped by σ_q and $-\sigma_q$ curves represent irradiance variability due to the water vapor variability given in Fig. 4.

Acknowledgements. This research was supported by the Agency for Defense Development (ADD), Korea, through the Image Information Research Center at Korea Advanced Institute of Science and Technology, and by the BK21 Program of the Korean Government.

REFERENCES

Anderson, G. P., and Coauthors, 2000: MODTRAN4: Radiative transfer modeling for remote sensing. *SPIE*, **4049,** 176–183.

Berk, A., and Coauthors, 1999: MODTRAN 4: Radiative transfer modeling for atmospheric correction. *SPIE*, **3756,** 348–353.

Goody, R. M., and Y. L. Yung, 1989: *Atmospheric Radiation: Theoretical Basis.* 2nd ed., Oxford University Press, New York, 519pp.

Hickey, M. P., 1988: *The NASA Marshall Engineering Thermosphere Model.* NASA CR 179389, 78pp.

Jacchia, L. G., 1970: *New Static Models of the Thermosphere and Exosphere with Empirical Temperature Profiles.* Smithsonian Astrophysical Observatory, Special Report 313, 154pp.

Justus, C. G., F. N. Alyea, D. M. Cunnold, W. R. Jeffries, and D. L. Johnson, 1991: The NASA/MSFC Global Reference Atmospheric Model-1990 Version (GRAM-90), Part I: Technical/Users Manual. NASA Technical Memorandum 4268, 76pp.

Justus, C. G., W. R. Jeffries III, S. P. Yung, and D. L. Johnson, 1995: The NASA/MSFC Global Reference Atmospheric Model - 1995 Version (GRAM-95). NASA Technical Memorandum 4715, 68pp.

Justus, C. G., and D. L. Johnson, 1999: The NASA/MSFC Global Reference Atmospheric Model: 1999 Version (GRAM-99), NASA Technical Memoradum TM-1999-209630, 153pp.

Kistler, R., and Coauthors, 2001: The NCEP-NCAR 50-year reanalysis: Monthly means CD-ROM and documentation. *Bull. Amer. Meteor. Soc.*, **82**, 247–268.

Kneizys, F. X., E. P. Shettle, L. W. Abreu, J. H. Chetwynd, G. P. Anderson, W. O. Gallery, J. E. A. Salby, and S. A. Clough, 1988: User Guide to LOWTRAN 7. Environ. Res. Papers, No. 1010, AFGL-TR-88-0177. Air Force Geophysical Laboratory, Hanscom, Massachusetts, 137pp.

Labitzke, K., J. J. Barnett, and B. Edwards, 1985: Middle atmosphere program-Atmosphere structure and its variation in the region 20 to 120 km-Draft of a new reference middle atmosphere. *Handbook for MAP*, **16**, 318pp.

Liou, K., 2002: *An Introduction to Atmospheric Radiation.* 2nd ed, Academic Press, 577pp.

McClatchey, R. A., R. W. Fenn, J. E. A. Selby, F. E. Volz, and J. S. Garing, 1972: Optical properties of the atmosphere. 3rd ed, AFCRL-72-0497, AD 753075. Air Force Geophysical Laboratory, L.G. Hanscom Field, Massachusetts, 108pp.

McCormick, M. P., and E. W. Chiou, 1994: Climatology of water vapor in the upper troposphere and lower stratosphere determined from SAGE II observations. 5th Global Change Studies, American Meteor. Soc., Nashville, TN, 23–28 January, 1994, 123–127.